Measurement of $\pi^- p$ Elastic Scattering at 14.15 GeV/c*

A. R. Dzierba, W. T. Ford, R. Gomez, P. J. Oddone, C. W. Peck, and C. Rosenfeld
California Institute of Technology, Pasadena, California 91109

and

R. P. Ely and D. F. Grether
Lawrence Berkeley Laboratory, Berkeley, California 94720

(Received 7 August 1972)

Results are presented of a wire-spark-chamber spectrometer measurement of the differential cross section for $\pi^- p$ elastic scattering at 14.15 GeV/c. The region covered in the square of the four-momentum transfer, t, is $0.01 < -t < 0.78$ (GeV/c)^2. The cross section is found to obey very nearly a simple exponential t dependence with no evidence of structure. A fit to the data of the form $d\sigma/dt \propto \exp(bt + ct^2)$ on the range $0.05 < -t < 0.78$ (GeV/c)^2 (i.e., above the region affected by Coulomb scattering) yields $b = 8.26 \pm 0.10$ (GeV/c)^2 and $c = 1.01 \pm 0.17$ (GeV/c)$^{-4}$. Considering the results of previous measurements, $b \simeq 11$ (GeV/c)$^{-2}$ for $-t < 0.05$ (GeV/c)^2, a deviation from the simple exponential near $-t \simeq 0.05$ (GeV/c)^2 is indicated.

I. INTRODUCTION

We present a measurement of the differential cross section for $\pi^- p$ elastic scattering at 14.15 GeV/c in the region $0.01 < -t < 0.78$ (GeV/c)^2. The data were obtained as a by-product of a hybrid wire-spark-chamber–bubble-chamber experiment designed to investigate diffractive production of nucleon isobars. Besides providing a calibration of the wire-spark-chamber system, the elastic scattering data constitute sufficiently detailed measurements to provide new information on the cross sections in this region of momentum transfer. In particular, the experiment is sensitive to possible small deviations in the angular dependence from the (approximately) exponential dependence previously observed.[1-3]

II. EXPERIMENTAL ARRANGEMENT

The experiment was performed by detecting the scattered pion from the reaction $\pi^- p \to \pi^- X$ and analyzing its momentum in a wire-spark-chamber magnetic spectrometer. The target was the Stanford Linear Accelerator Center (SLAC) 40-in. bubble chamber filled with liquid hydrogen.

A 14-GeV negative beam was produced at 1° with respect to the incident electrons in a beryllium target in the central beam line of End Station B, and was transported through two intermediate foci to the bubble chamber. A 1-radiation-length lead filter at the first focus followed by momentum redefinition at the second served to remove the large electron contamination. The momentum was defined to within ±0.31%. The residual contaminations in the π^- beam were electrons, 2.4%; K^-, 1%; μ^-, several percent. Transverse beam dimensions at the bubble chamber were 0.25 in. × 5 in., the one large dimension being required to spread the tracks as viewed by the bubble-chamber cameras. The beam angular dimensions were ±1.4 mrad × ±0.6 mrad. Typically, the beam rate was 9 pions per SLAC pulse, the pulse length being 1.6 μsec, at repetition rates of 3–5 per second.

Figure 1 is a diagram of the experiment layout. Pions scattered through small angles in the bubble chamber passed through the exit windows and traversed four wire-spark-chamber measuring stations, two before and two after the 40D48 (40 in. wide × 15 in. high × 48 in. long) magnet. Each station consisted of two magnetostrictive wire chambers, each having x and y readout. An additional pair of chambers at station 1 was oriented at 45° to provide information sufficient for unique matching of the two views. The active areas of stations 1 and 3 were covered by $\frac{1}{8}$ in.-thick scintillators, and coincidences in these counters constituted a trigger for the spark chambers. Both the scintillators and the wire chambers were insensitive in the area traversed by the beam, a region about ±5 mrad wide and extending the full height of the detectors.

This system with its readout was designed to provide very fast on-line reconstruction of the scattered tracks: a Sigma 2 computer returned a decision to trigger the bubble-chamber lights within the 3 millisecond bubble-growth delay. A trigger was indicated whenever a track was found which was consistent with an inelastic scatter in the bubble chamber. The raw spark-chamber data were, however, recorded on magnetic tape whenever a spark-chamber trigger occurred, so that elastic scatters are also present in the spectrometer data sample.

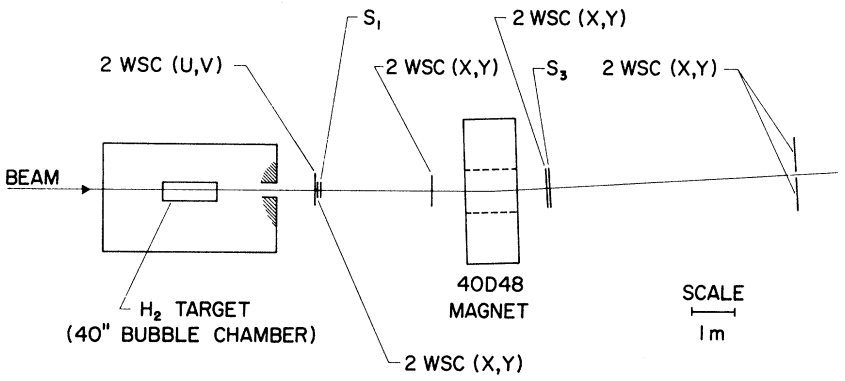

FIG. 1. Plan view of the experiment. The bubble chamber is represented by the outline of the hydrogen vessel and of the surrounding magnet. The bubble-chamber magnetic field is perpendicular to the beam in the plane of the drawing.

The spectrometer angular acceptance covered horizontal scattering angles $5 < |\theta_x| < 60$ mrad and vertical angles $0 < |\theta_y| < 20$ mrad. This implies a range in four-momentum transfer squared (t) of $0.01 < -t < 0.78$ (GeV/c)^2, with a t-dependent acceptance averaging about 60% for elastic and low-mass inelastic events. The difference in momentum between incoming and scattered pion was measured with a precision of ± 70 MeV/c, which implies a resolution in missing mass of ± 70 MeV near the elastic peak. The outgoing angle was measured within ± 0.15 mrad, so the dominant error on the scattering angle for events having no bubble-chamber information was the angular spread of the incident beam.

A total of 4.1×10^5 elastic scatters were recorded during the experiment, together with a slightly smaller number of inelastic events of which bubble chamber pictures were taken. Analysis of the bubble-chamber data is in progress. We describe in the following section the analysis of the spark-chamber data as it applies to the elastic events.

III. DATA ANALYSIS

The spark-chamber raw data were searched for tracks by first combining the data from the two adjacent chambers at each station into a single list, then searching the four lists for combinations consistent with two track segments intersecting at the magnet center. (In the elevation view there occurs only a small bend due to edge focusing in the magnet.) A spark in the diagonal chambers was required to establish the correspondence between the two views whenever more than one choice existed. The use of redundant pairs of chambers at each station insured high efficiency while permitting a simple matching algorithm for the on-line bubble-chamber trigger program.

The missing mass recoiling against the detected π^- was computed from the fitted tracks and the resulting distribution is shown in Fig. 2. The elastic peak has an rms width of ± 70 MeV. The centroid of this peak was used to calibrate the momentum scale, which showed run-to-run drifts of ~25 MeV. A sample of elastic events was selected by cutting the corrected spectra at 600 < missing mass < 1225 MeV. It is estimated that 2% of the elastics were removed by this cut, and a comparable contamination of inelastics was accepted. Other cuts included a requirement that the confidence level of the track fit exceed 1.5% (resulting in a loss of 1.5% of the data), and a cut on the horizontal projection of the scattering angle, $|\theta_x| > 5$ mrad, which amounted to

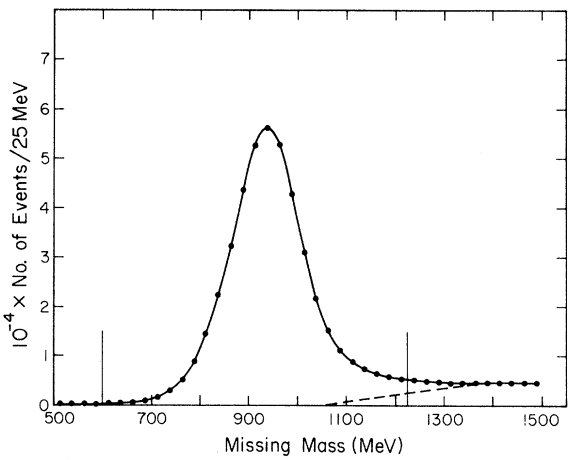

FIG. 2. The missing-mass spectrum, uncorrected for the apparatus acceptance. The dashed curve indicates the contribution of inelastic events, estimated from the spectra of Ref. 3. The cuts used to define the elastic events are indicated.

TABLE I. Results for the differential cross section for $\pi^- p \to \pi^- p$ at 14.15 GeV/c. The errors given in the table are statistical. There is an additional normalization uncertainty of ±6%.

$-t$ [(GeV/c)^2]	$d\sigma/dt$ [mb (GeV/c)$^{-2}$]	Error	$-t$ [(GeV/c)^2]	$d\sigma/dt$ [mb (GeV/c)$^{-2}$]	Error
0.015	30.42	±0.783	0.250	4.474	±0.0911
0.025	25.21	±0.490	0.270	3.826	±0.0858
0.035	24.29	±0.320	0.290	3.195	±0.0810
0.045	22.50	±0.275	0.310	2.803	±0.0770
0.055	20.17	±0.260	0.330	2.269	±0.0805
0.065	18.93	±0.234	0.350	1.990	±0.0752
0.075	17.43	±0.226	0.375	1.690	±0.0483
0.085	16.20	±0.214	0.405	1.357	±0.0471
0.095	14.82	±0.203	0.435	1.055	±0.0390
0.105	13.68	±0.192	0.465	0.9108	±0.0358
0.115	12.48	±0.193	0.495	0.7038	±0.0335
0.125	11.72	±0.189	0.525	0.5505	±0.0266
0.135	10.87	±0.177	0.555	0.4674	±0.0266
0.145	10.00	±0.167	0.585	0.3253	±0.0318
0.155	8.846	±0.175	0.615	0.2992	±0.0177
0.165	8.595	±0.154	0.645	0.2280	±0.0164
0.175	7.655	±0.162	0.675	0.2182	±0.0184
0.185	7.531	±0.146	0.705	0.1712	±0.0186
0.195	6.728	±0.161	0.735	0.1084	±0.0193
0.210	5.692	±0.108	0.765	0.1351	±0.0278
0.230	5.118	±0.0951			

a trim of the beam dead region cutoff of the detectors and served to remove muon tracks from the sample. The number of events removed by this cut was 1.4%.

The angular distribution was obtained from the histogram of the raw data by subtracting the target-empty counts (7% of target-full) and correcting each bin for (1) the acceptance of the apparatus, obtained from a Monte Carlo calculation, and (2) the calculated effect of double elastic scattering in the target.

The differential cross section $d\sigma/dt$ is given by the angular distribution normalized by the number of counts in the beam counter and the number of target protons, and corrected for a normalization factor for the beam counter, which suffered dead-time losses (−11%), dead-time losses in the scattered particle detectors (+13%), nuclear absorption in the target (10%), loss of events due to cuts (+2%), contamination of inelastics and accidental fits (−2%), efficiency of the spark chambers (+2.5%), nuclear absorption in the spectrometer (+1%), and decay of the scattered pions (+1%). The over-all normalization is uncertain within ±6%, the principal contributions to this error arising from the beam count and the dead-time correction.

A small distortion of the t distribution is caused by the t-dependent resolution uncertainty in the value of t. This uncertainty, due to the angular spread of the incident beam, is given by $\Delta t_{\rm rms} = 2p\Delta\theta\sqrt{-t} = 0.034\sqrt{-t}$. The effect on an exponential

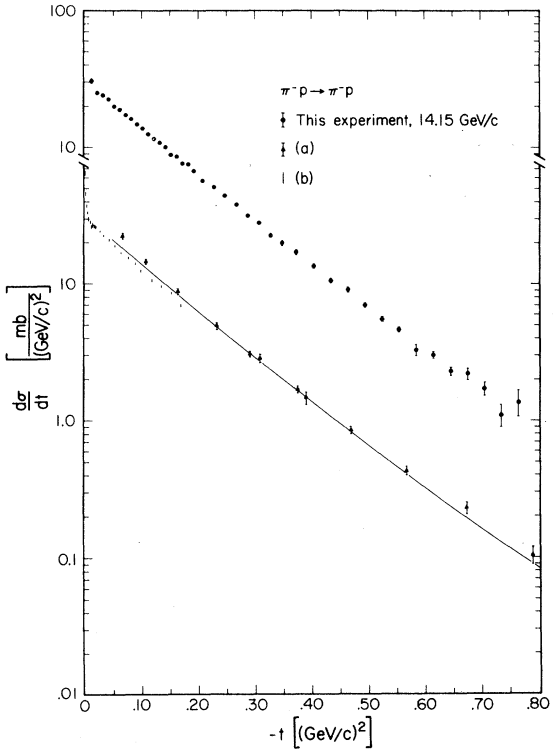

FIG. 3. Results of the measurement of $d\sigma/dt$. The ±6% normalization uncertainty is not indicated. Also shown are the results (a) of Ref. 1 at 15 GeV/c, and (b) of Ref. 4 at 16 GeV/c. The curve accompanying these points is a fit to our data for comparison.

TABLE II. The results of fits to $d\sigma/dt$. b corrected includes an added term +0.04 $(\mathrm{GeV}/c)^{-2}$ due to the t resolution. DF=degrees of freedom.

	Linear fit $d\sigma/dt = \exp(a + bt)$				Quadratic fit $d\sigma/dt = \exp(a + bt + ct^2)$				
$-t$ range $[(\mathrm{GeV}/c)^2]$	a	b $[(\mathrm{GeV}/c)^{-2}]$	χ^2 (DF)	b corrected $[(\mathrm{GeV}/c)^{-2}]$	a	b $[(\mathrm{GeV}/c)^{-2}]$	c $[(\mathrm{GeV}/c)^{-4}]$	χ^2 (DF)	b corrected $[(\mathrm{GeV}/c)^{-2}]$
0.01–0.78	3.434 ± 0.005	7.74 ± 0.03	95.3 (39)	7.78 ± 0.03	3.474 ± 0.008	8.28 ± 0.08	1.09 ± 0.15	43.5 (38)	8.32 ± 0.08
0.01–0.30	3.456 ± 0.006	7.95 ± 0.05	37.8 (22)	7.99 ± 0.03	3.480 ± 0.012	8.41 ± 0.19	1.63 ± 0.66	31.6 (21)	8.45 ± 0.19
0.05–0.78	3.419 ± 0.006	7.68 ± 0.03	65.2 (35)	7.72 ± 0.03	3.467 ± 0.010	8.22 ± 0.10	1.01 ± 0.17	31.6 (34)	8.26 ± 0.10
0.05–0.30	3.444 ± 0.008	7.88 ± 0.06	21.9 (18)	7.92 ± 0.06	3.468 ± 0.020	8.25 ± 0.29	1.17 ± 0.90	20.0 (17)	8.29 ± 0.29
0.05–0.18	3.458 ± 0.013	8.03 ± 0.12	7.7 (11)	8.07 ± 0.12	3.427 ± 0.040	7.39 ± 0.78	−2.91 ± 3.51	7.8 (10)	7.43 ± 0.78

t distribution is to reduce the observed logarithmic slope. The correction, applied after fitting the cross section to the form Ae^{bt}, is given by $b = b_{\mathrm{fit}}(1 + 0.58 \times 10^{-3} b_{\mathrm{fit}})$, which for $b \simeq 8$ adds ~ 0.04 to b.

IV. RESULTS

Results for the $\pi^- p$ elastic scattering cross section are presented in Table I and Fig. 3. The bin widths have been chosen to be comparable to the resolution in t. The errors quoted are statistical. In addition, an over-all systematic normalization error of ±6% applies.

The cross section has a smooth, nearly exponential dependence upon t over the full range of the measurements. The results of fits of $\ln(d\sigma/dt)$ to linear and quadratic functions spanning various ranges of t are given in Table II. The table shows that the data for $-t < 0.3$ $(\mathrm{GeV}/c)^2$ fit a single exponential, particularly if the region $-t < 0.05$ $(\mathrm{GeV}/c)^2$ is excluded (see Sec. V). Over the full range $-t < 0.78$ $(\mathrm{GeV}/c)^2$ a small quadratic term is required.

In Table II, the column labeled "b corrected" gives the slope corrected as described above for the small shift caused by the resolution in t.

V. DISCUSSION

For comparison with our data we have included in Fig. 3 the results of two earlier experiments of Foley *et al.*[1,4] at nearby beam energies. The cross section we measure is quite similar to the low-t data of Ref. 4. Our data show slightly less curvature as a function of t than those of Ref. 1. Anderson *et al.*[3] have also measured the logarithmic slope of the cross section at 16 GeV/c. These authors quote the result $b = 7.8 \pm 0.3$ $(\mathrm{GeV}/c)^{-2}$, in good agreement with our value $b = 7.92 \pm 0.06$ $(\mathrm{GeV}/c)^{-2}$ in this region.

Indications of breaks at low t in the cross sections for this and other reactions, notably pp elastic scattering, have been pointed out by Carrigan[5] and more recently have been observed in pp scattering at the CERN Intersecting Storage Rings.[6] Our data show no evidence of any break above $-t \simeq 0.05$ in $\pi^- p$ at 14 GeV.

With the aid of Fig. 4 we examine in more detail the low-t region. Shown there are our data together with the 16.00 GeV/c measurements from Ref. 4. Foley *et al.*[4] have made fits to their data for $-t < 0.05$ to an expression for the cross section that includes the Coulomb and Coulomb-nuclear interference terms. The resulting fitted curve for the nuclear part has been drawn in the figure, together with curves showing exponential fits above $-t = 0.05$ both to our data ($0.05 < -t < 0.18$) and to those

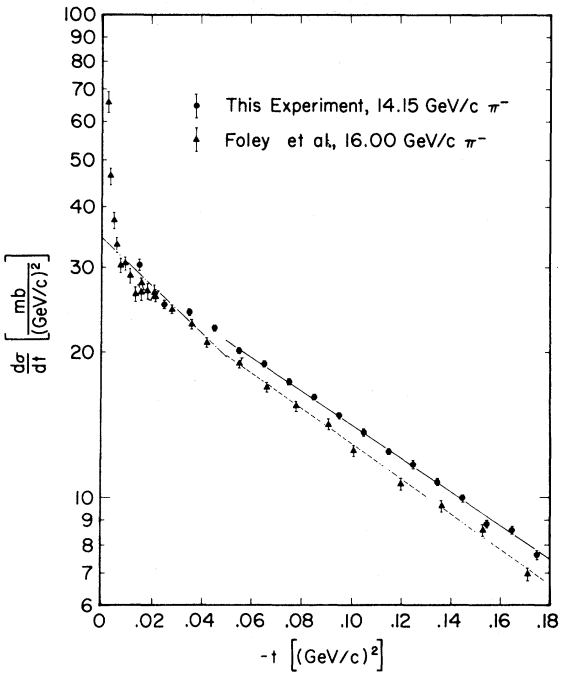

FIG. 4. Results of this experiment and of Ref. 4 in the small $|t|$ region. The solid curve is an exponential fit to our data for $0.05 < -t < 0.3$ $(\mathrm{GeV}/c)^2$. The dashed curve is an exponential fit to the data of Ref. 4 for $-t > 0.05$ $(\mathrm{GeV}/c)^2$. The dot-dashed curve represents the hadronic part of the expression fit by Foley *et al.* (Ref. 4) to their data for $-t < 0.05$. The deviation of the points from this curve is due to the Coulomb interaction.

of Ref. 4. The logarithmic slopes are 8.07 ± 0.12 and 8.35 ± 0.23, respectively. (The normalization difference between the two sets of measurements is well within the assigned uncertainties.) The slope below $-t = 0.05$, on the other hand, is 11.12 ± 0.32,[4] a significantly higher value. This larger value is typical of the fits obtained in this range for various beam energies.[4,5]

We conclude that (1) from our data the cross section is within small errors a simple exponential function of t above the Coulomb interference region, with no evidence of any break. The logarithmic slope is about 8 $(\mathrm{GeV}/c)^{-2}$. (2) From the data of Ref. 4, the hadronic part of the cross section below $-t = 0.05$ is a steeper function of t, the logarithmic slope being between 10 and 11 $(\mathrm{GeV}/c)^{-2}$. (3) The two experiments are in good agreement in the region in which they overlap. Apparently the $\pi^- p$ cross section near 15 GeV has a break at $-t \simeq 0.05$.

The optical theorem value for $d\sigma/dt|_{t=0}$ at our energy is 34.8 mb $(\mathrm{GeV}/c)^{-2}$, derived from the measured value[7] of $\sigma_{\mathrm{tot}} = 25.915 \pm 0.081$ mb at 14.13 GeV/c, and from the measured ratio[4] of the real to imaginary parts of the scattering amplitude, $\mathrm{Re}f/\mathrm{Im}f|_{t=0} = -0.113 \pm 0.025$ at 14.16 GeV/c. If our fit to $d\sigma/dt$ is extrapolated to $t = 0$, the normalization factor required to bring our data into agreement with the optical theorem is 1.08. If instead we assume the slope parameter changes abruptly to 10.5 $(\mathrm{GeV}/c)^{-2}$ at $-t = 0.05$, the factor becomes 0.97. In either case the factor is consistent with unity within our normalization error of ± 0.06.

ACKNOWLEDGMENT

We would like to thank the staff of the Stanford Linear Accelerator Center for their support in setting up the experiment and for the excellent operation of the accelerator. In particular, we thank Dr. J. J. Murray for his very substantial assistance both in designing the beam and in making it operational.

*Work supported in part by the U. S. Atomic Energy Commission and prepared under Contract No. AT(11-1)-68 for the San Francisco Operations Office, U. S. Atomic Energy Commission.

[1]K. J. Foley *et al.*, Phys. Rev. Letters 11, 425 (1963).
[2]K. J. Foley *et al.*, Phys. Rev. Letters 15, 45 (1965).
[3]E. W. Anderson *et al.*, Phys. Rev. Letters 25, 699 (1970).
[4]K. J. Foley *et al.*, Phys. Rev. 181, 1775 (1969).
[5]R. A. Carrigan, Jr., Phys. Rev. Letters 24, 168 (1970).
[6]G. Barbiellini *et al.*, Phys. Letters 39B, 663 (1972).
[7]K. J. Foley *et al.*, Phys. Rev. Letters 19, 330 (1967).